Favorable recycling photocatalyst TiO$_2$/CFA: Effects of calcination temperature on the structural property and photocatalytic activity

Jian-wen Shi*, Shao-hua Chen*, Shu-mei Wang, Zhi-long Ye, Peng Wu, Bin Xu

Key Laboratory of Urban Environment and Health, Institute of Urban Environment, Chinese Academy of Sciences, No. 1799, Jimei Road, Xiamen, Fujian 361021, China

ABSTRACT

A batch of TiO$_2$/CFA photocatalysts was prepared by using coal fly ash (CFA), waste discharged from coal-fired power plant, as substrate. The effects of calcination temperature on the structural property of TiO$_2$/CFA, such as morphology, crystal structure, porous property and light absorption characteristic were investigated in detail. Further more, the effects of calcination temperature on the photocatalytic activity and the recycling property of TiO$_2$/CFA were studied by the photocatalytic decoloration and mineralization of methyl orange solution. The results show that calcination temperature affected the photocatalytic activity and the recycling property of TiO$_2$/CFA by many ways: the increase in calcination temperature can improve the crystallization of TiO$_2$, decrease the specific surface area of TiO$_2$/CFA, promote the grain growth of TiO$_2$, and can enhance the mechanical stability of TiO$_2$/CFA in the range of 400–700 °C. 700 °C is the optimum calcination temperature for obtaining the optimal photocatalytic activity and re-use property of TiO$_2$/CFA under the conditions investigated in this study.

© 2010 Elsevier B.V. All rights reserved.

1. Introduction

TiO$_2$ has been attracting much attention in view of its advantage as a photocatalyst to eliminate environmental pollutions such as water treatment, air purification and bacteria inactivation [1–3]. Degussa P25 is extensively used as a standard in photocatalysis [4–5]. However, one of the main problems limited the practical applications of P25 in water treatment is that the nano-meter TiO$_2$ particles in aqueous suspension are very difficult to be separated from water after use [6–8]. Therefore, many materials have been proposed for the immobilization of TiO$_2$ to eliminate this problem. Glass [9–11], zeolite [12,13], silica [14,15], activated carbon [16,17], etc. have been used as substrates by some scholars for the immobilization of TiO$_2$.

Coal fly ash (CFA) is one of the solid wastes largely produced from coal-fired power plant [18,19]. In our early publication [20], we immobilized TiO$_2$ on the surface of CFA successfully by employing three kinds of approaches, and we found the hybrid slurry procedure was a more proper method to immobilize TiO$_2$ on CFA than the other two procedures because the TiO$_2$/CFA sample prepared by hybrid slurry procedure exhibited higher photocatalytic activity and better repeatability. But the effects of calcination temperature on the photocatalytic activity of TiO$_2$/CFA sample have not been investigated in that work because they were not the

focus of that article. In fact, many studies have confirmed that the photocatalytic activity of TiO$_2$ was greatly affected by calcination temperature [21–23]. However, the effects of calcination temperature on the structural property and photocatalytic activity of TiO$_2$/CFA have not yet been reported. So, in current work, we prepared a batch of TiO$_2$/CFA photocatalysts calcined at different temperature by the same method (hybrid slurry procedure) described in our early article [20], and the effects of calcination temperature on the structural property of TiO$_2$/CFA, such as morphology, crystal structure, porous property and light absorption characteristic were investigated in detail. Further more, the effects of calcination temperature on the photocatalytic activity and the recycling property of TiO$_2$/CFA were investigated by the photocatalytic decoloration and mineralization of methyl orange (MO) solution.

2. Experimental

2.1. Preparation of TiO$_2$/CFA

All TiO$_2$/CFA samples were prepared by hybrid slurry procedure described in our early article [20]. The loading percent of TiO$_2$ was 28.54, 37.47, 44.41, 49.97 and 54.51%, respectively (the loading percent of TiO$_2$ (L_p) calculated by using Eq. (1)). The calcination temperature was 400, 500, 600, 700, and 800 °C, respectively. For convenience, we used a, b, c, d and e to represent the loading percent of 28.54, 37.47, 44.41, 49.97% and 54.51%, respectively, and we denoted these TiO$_2$/CFA samples as TiO$_2$/CFA-(loading percent

* Corresponding authors. Tel.: +86 592 6190528; fax: +86 592 6190977.
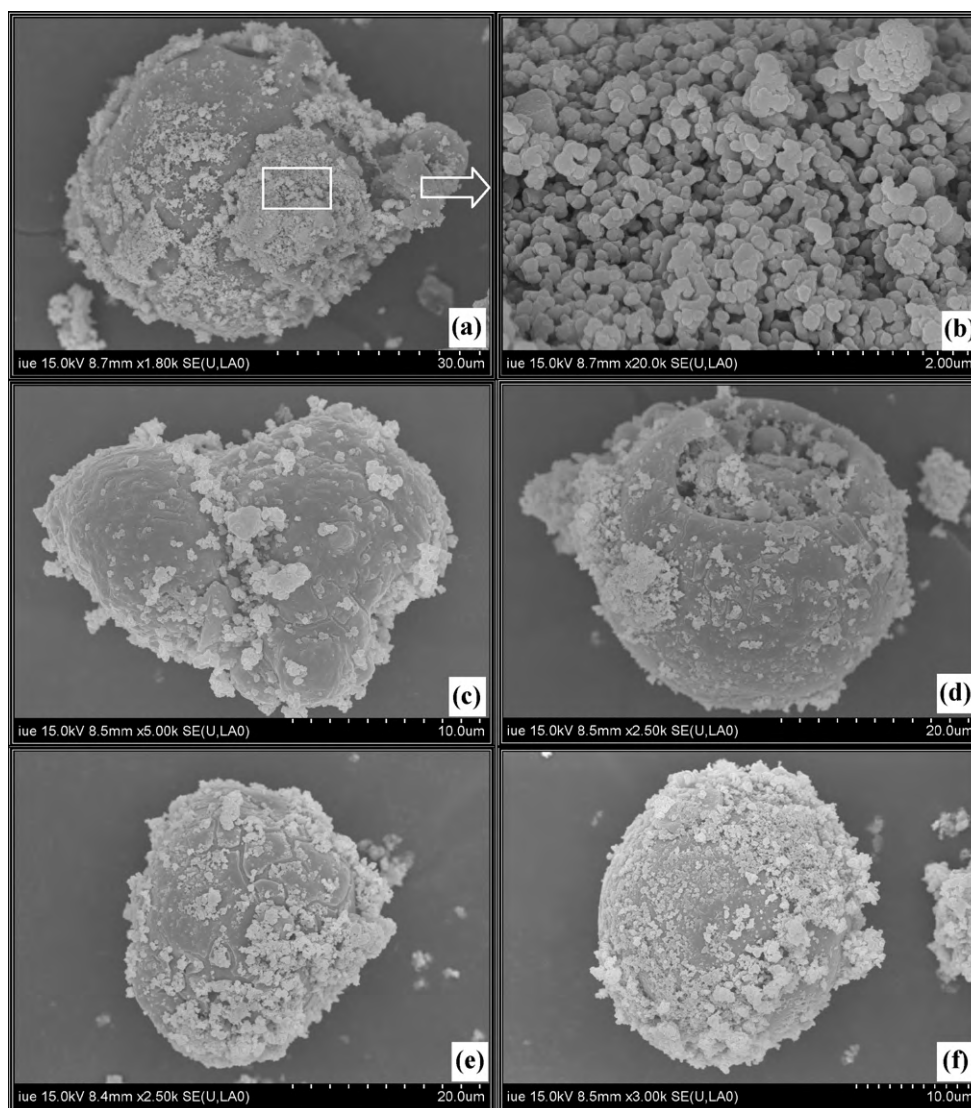*E-mail addresses:* shijnwn@163.com (J.-w. Shi), shchen@iue.ac.cn (S.-h. Chen).

Fig. 1. SEM images of TiO$_2$/CFA samples: (a) TiO$_2$/CFA-d400; (b) the local enlargement of (a); (c) TiO$_2$/CFA-d500; (d) TiO$_2$/CFA-d600; (e) TiO$_2$/CFA-d700; (f) TiO$_2$/CFA-d800.

of TiO$_2$) (calcination temperature). For example, if a sample was loaded with 28.54% TiO$_2$ and calcined at 400 °C, it was marked as TiO$_2$/CFA-a400:

$$L_p(\%) = \frac{100 W_{TiO_2}}{W_{TiO_2} + W_{CFA}}(\%) \qquad (1)$$

where W_{TiO_2} is the weight of TiO$_2$, and W_{CFA} is the weight of CFA.

2.2. Characterizations

The morphology of samples was observed by scanning electron microscope (SEM, S-4800, Japan). X-ray diffraction (XRD) pattern of samples was obtained at room temperature using a diffractometer (X'pert PROMPD, Holand) with copper Kα radiation. The nitrogen adsorption–desorption isotherms at 77 K were obtained by using a Gas Absorption Analyzer (Micromeritics TriStar 3000, America), and the pore size distribution and specific surface area were calculated according to BJH and BET model, respectively. Ultraviolet–visible (UV–vis) absorption spectroscopy of samples was recorded by a spectrophotometer (Shimadzu UV-2450, Japan) equipped with an integrating sphere, and the baseline correction was done using a calibrated sample of barium sulfate. The absorbance of MO solution was measured by using a spectropho-

tometer (SpectraMax M5, China) at the wavelength of 465 nm. The total organic carbon (TOC) concentration was determined by using a Total Organic Analyzer instrument (Shimadzu, TOC-V CPH, Japan).

3. Results

3.1. SEM analysis

The effects of calcination temperature on the surface morphology of TiO$_2$/CFA samples were characterized by SEM and the results are illustrated in Fig. 1 (the micrograph of CFA has been shown in our previous publication [20]). It can be observed from Fig. 1(a), due to the low calcination temperature, the structure of TiO$_2$ adhered to CFA looks very fluffy, which is disadvantaged in extending the use-life of TiO$_2$/CFA photocatalyst because the TiO$_2$ particles are easy to break away from the surface of CFA in the course of use, and the photocatalytic activity of TiO$_2$/CFA will be lost gradually. From Fig. 1(b), the local enlargement of Fig. 1(a), we can see that a three-dimensional (3D) network structure has appeared which can significantly increase the surface area and adsorption capacity of sample. From the SEM images (Fig. 1(c)–(e)), we can see that, except for granular TiO$_2$ adhered on CFA, CFA microsphere has been wrapped in a layer of TiO$_2$ film, and some cracks appear in TiO$_2$ film
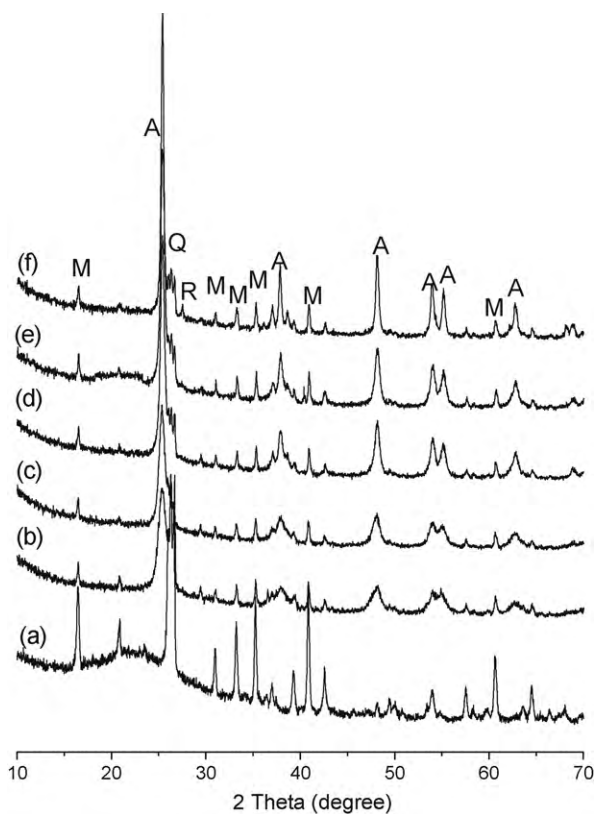
Fig. 2. XRD patterns of CFA and TiO_2/CFA samples (M: mullite; Q: quartz; A: anatase; R: rutile): (a) CFA; (b) TiO_2/CFA-d400; (c) TiO_2/CFA-d500; (d) TiO_2/CFA-d600; (e) TiO_2/CFA-d700; (f) TiO_2/CFA-d800.

due to the shrinkage of film during heat treatment. When calcination temperature further ascends to 800 °C, many flakes of TiO_2 film have appeared, and seemed to fall off from the surface of CFA (Fig. 1(f)).

3.2. XRD analysis

Fig. 2 shows the XRD patterns of CFA and TiO_2/CFA samples calcined at 400, 500, 600, 700 and 800 °C for 2 h, respectively. The XRD pattern of CFA shows that CFA contains quartz and mullite in large amount [24]. After TiO_2 was loaded on CFA, the intensity of diffraction peaks correlated with quartz and mullite becomes weak gradually (for instance, the peak appeared at $2\theta = 26.08°$ is the diffraction peak of quartz [24]), while the diffraction peaks of the anatase TiO_2 begin to appear in XRD patterns. TiO_2 in TiO_2/CFA-d400 sample presents only the anatase phase, with wide diffraction peaks indicating low crystallization [25]. With the ascent in calcination temperature, the peak intensity of anatase phase increases significantly (such as the peak appeared at $2\theta = 25.4°$, which is the 1 0 1 plane of anatase TiO_2 [26–28]), indicating the improvement in crystallization of anatase phase [29–31]. Simultaneously, the width of the (1 0 1) peak becomes narrower, suggesting the growth of anatase crystallites [30,31]. When the calcination temperature increases to 800 °C, a minor but discernible peak at $2\theta = 27.45°$ appears, which is assigned to rutile phase [28,32,33]. This indicates that the phase transformation temperature of anatase to rutile is 800 °C after TiO_2 was anchored on CFA. Usually, for pure TiO_2 samples, the rutile phase starts to appear at 600–700 °C [34,35], implying that CFA inhibits the phase transformation of TiO_2. The average crystal size of anatase TiO_2 was estimated to the full width at half-maximum (FWHM) of the (1 0 1) peak of anatase by applying

Table 1
Calculation results of crystal size, surface area and adsorption ratio.

Sample	Crystal size (nm)	S_{BET} (m²/g)	MO adsorption ratio (%)
CFA	nd[a]	0.4	nd[a]
P25	24.7	53.3	15.3
TiO_2/CFA-d400	11.5	64.0	25.9
TiO_2/CFA-d500	38.4	32.0	19.9
TiO_2/CFA-d600	57.6	13.0	13.5
TiO_2/CFA-d700	85.5	12.6	13.1
TiO_2/CFA-d800	116.9	4.1	3.1

[a] Not determined.

the Scherrer equation as follows [36,37]:

$$D = \frac{K\lambda}{\beta \cos\theta} \tag{2}$$

where K is a constant (shape factor, about 0.89), λ is the X-ray wavelength, β is the FWHM of the diffraction line, and θ is the diffraction angle. The results are presented in Table 1 (the crystal size of anatase in P25 is also presented as a reference). We can see from the table that, with the increase in calcination temperature, the crystal size of TiO_2 increases gradually. When the calcination temperature rises to 800 °C, an obvious increase in the crystal size occurs because of the phase transformation from anatase to rutile. Usually, the increase in calcination temperature can accelerate the growth of crystallites and induce phase transformation from anatase to rutile [38]. Many other researchers also found that the average crystal size increased with the increase in calcinations temperature, in good agreement with our present results [39–41].

3.3. Nitrogen adsorption test

Fig. 3 shows the nitrogen adsorption–desorption isotherms of CFA and TiO_2/CFA samples calcined at various temperature. CFA shows an isotherm of type II and no hysteresis, referring to non-porous material [42]. The isotherm of the TiO_2/CFA samples calcined in the range from 400 to 700 °C reveals a typical type IV sorption behavior, representing the predominant mesoporous structure characteristic according to the classification of IUPAC [31,43]. When the calcination temperature reaches to 800 °C, the hysteresis loop of sample is difficult to be observed, which is probably attributed to the collapse of 3D network structures in the TiO_2/CFA sample during calcination [30,32]. The isotherms shown in Fig. 3 also suggest that the pore volume decreases with the increase in calcination temperature, which indicates that thermal
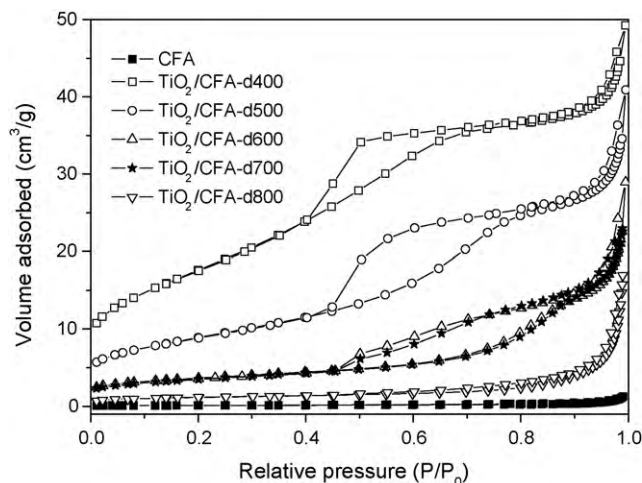

Fig. 3. Nitrogen adsorption–desorption isotherms of CFA and TiO_2/CFA samples.
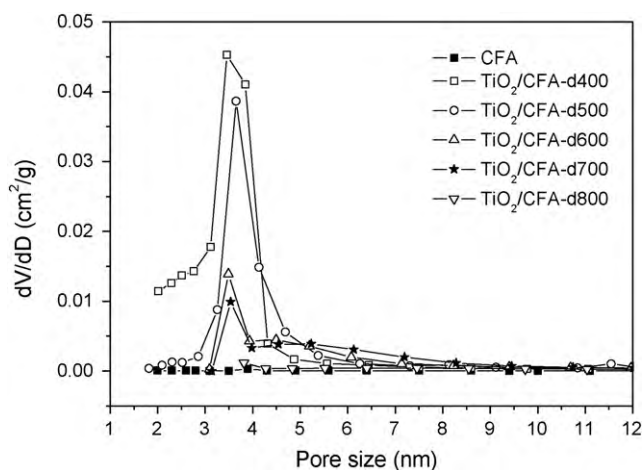
Fig. 4. Pore size distributions of CFA and TiO$_2$/CFA samples.

treatment will decrease the specific surface area (S_{BET}) and the pore volume of TiO$_2$/CFA samples simultaneously [31]. Table 1 shows the S_{BET} of all samples calculated by Brunauer–Emmett–Teller (BET) method. It can be seen that the calcination temperature produces a significant decrease in the S_{BET} of TiO$_2$/CFA samples [25]. Many other researchers also found the same phenomenon that the S_{BET} decreased with the increase in calcination temperature [30,39].

The pore size distributions of all samples are displayed in Fig. 4. It can be observed that, except for CFA no pore, a certain amount of the mesoporous structure have been formed in all TiO$_2$/CFA samples, and the mesoporous structure decreases with the increase in calcination temperature, indicating that the pore size distributions of the TiO$_2$/CFA samples strongly depend on the calcination temperature.

3.4. UV–vis absorption spectroscopy

Information about the light absorption characteristic of samples can be obtained from UV–vis absorption spectroscopy. This is very important property for photocatalytic application as catalyst since it gives information about the band gap of semiconductor [25]. The UV–vis absorption spectroscopies of TiO$_2$/CFA samples calcined at different temperature are presented in Fig. 5. In order to compare, CFA and P25 were also measured at the same conditions. It can be seen that CFA, with the color of gray, exhibits strong absorption in
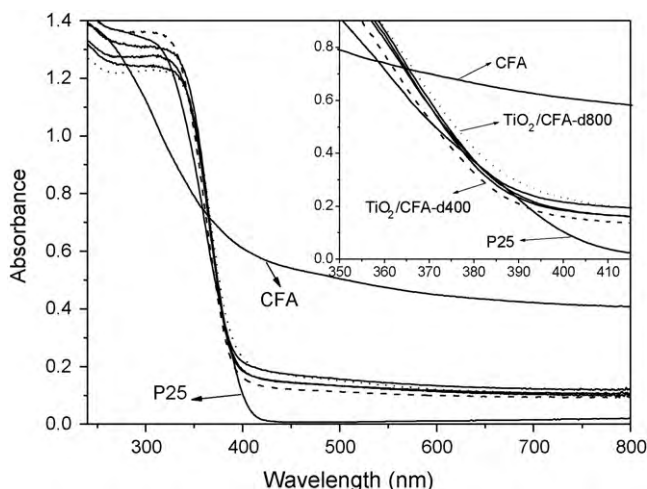

Fig. 5. UV–vis absorption spectroscopy of samples.

whole range of wavelength employed. All of the spectrums (except for CFA) clearly show the characteristic absorption edge of semiconductor TiO$_2$. The absorbance of TiO$_2$/CFA samples in the region of visible light starting at around 400 nm is better than P25. Further observation shows that the absorption edges of the TiO$_2$/CFA samples increase with the increase in calcination temperature, which is probably attributed to the fact that the increase in crystal size can cause red shift of absorption edge [38,44]. Red-shift extent of the sample calcined at 800 °C is the biggest among these samples, which is probably ascribed to the fact that the part phase transforms from anatase to rutile leads to the decrease of band gap [36,38,44].

3.5. Adsorption property

The adsorption property of MO on the TiO$_2$/CFA samples calcined at different temperatures was measured in the dark under the same conditions as UV irradiation. Such adsorption investigation for TiO$_2$/CFA samples can provide information of the actual effective surface area in the photocatalyst that can be utilized for adsorption of organic pollutants in water and may have an advantage over nitrogen adsorption test of samples [33]. The adsorption experiment lasted 30 min to ensure the adsorption equilibrium was reached. The decoloration ratio of MO due to the adsorption of TiO$_2$/CFA samples is shown in Table 1. From the table, we can see that adsorption ratio increases with the increase in S_{BET}, at the same time, the S_{BET} of sample decreases with the increase in calcination temperature. That is to say, the adsorption capacity of sample decreases with the increase in calcination temperature. A number of earlier reports [33,45] have also shown that adsorption property of catalyst decreases with the increase in calcination temperature.

3.6. Photocatalytic activity

The photocatalytic activity of all samples was measured by the decoloration ratio of MO solution without concerning the degradation intermediates in detail. The photo reactor system and experimental procedures were the same as what described in our previous article [20]. The decoloration ratio of MO solution versus photocatalytic time under mercury lamp irradiation is shown in Fig. 6. We can conclude a uniform rule from Fig. 6 that the photocatalytic activity of TiO$_2$/CFA can be improved by enhancing the calcination temperature in the range from 400 to 700 °C. However, the photocatalytic activity of TiO$_2$/CFA sample decreases significantly when calcination temperature further increases to 800 °C.

Comparing with all TiO$_2$/CFA samples, P25 is more effective to perform the decoloration of MO solution. But the precipitation property of P25 is very poor (see Fig. S1 shown in the Supporting Information in our previous publication [20]), so the particle filtration is needed in order to separate P25 powders from the treated water. TiO$_2$/CFA samples have a good precipitation property and can be separated from the treated wastewater by precipitating in a quiescent condition for some time because of the heavy weight of CFA, which has also be proved by our previous experiment shown in the Supporting Information [20]. So we think that it is worthy to obtain a simple method of recycling catalyst by sacrificing the photocatalytic performance of catalyst in a certain extent.

3.7. Re-use property

The main purpose loading TiO$_2$ on CFA is to improve the re-use property of photocatalyst, then, how about the recycling property of the TiO$_2$/CFA photocatalyst? In order to answer this question, we designed the recycle experiment on the photocatalytic decoloration of MO solution. The experimental procedures were the same as what described in our previous article [20]. Fig. 7 dis-
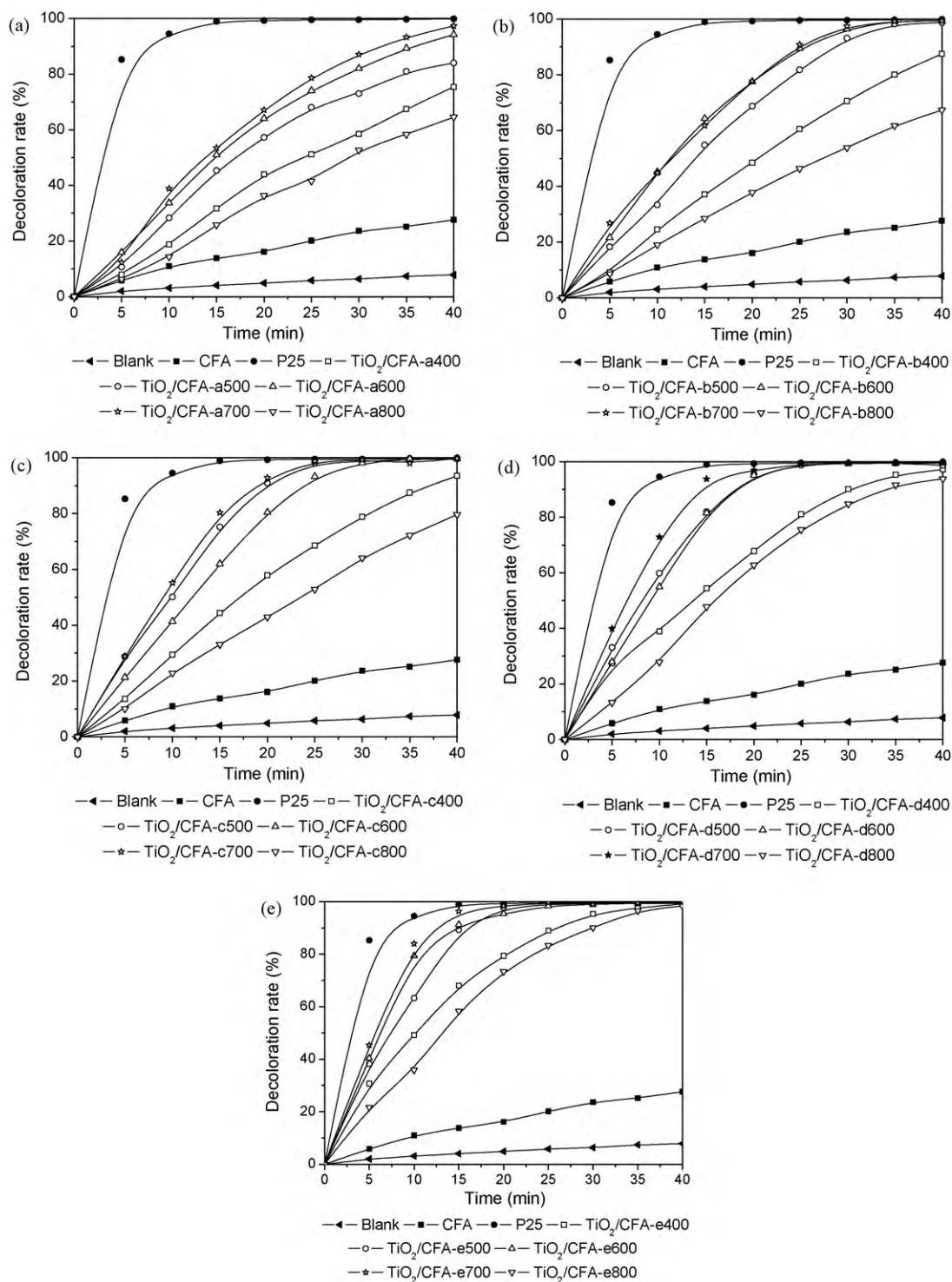
Fig. 6. Decoloration curves of MO solution by samples calcined at different temperature and loaded with different amount of TiO_2: (a) 28.54%; (b) 37.47%; (c) 44.41%; (d) 49.97%; (e) 54.51%.

plays the results of the decoloration ratio versus cycle times. It can be observed that the decoloration ratio is degressive with the increase in cycle times when TiO_2/CFA-d400 or TiO_2/CFA-d800 is used as photocatalyst. The other three photocatalysts (TiO_2/CFA-d500, TiO_2/CFA-d600 and TiO_2/CFA-d700) always keep a high photocatalytic activity, and the efficiency of photocatalytic decoloration is maintained without significant decline when they are used repeatedly, even at the sixth cycle. These phenomena show that, comparing with the photocatalysts calcined at 400 and 800 °C,

the photocatalysts calcined at 500, 600 and 700 °C have a better re-use performance.

3.8. Mineralization of MO

The ultimate products of the photocatalytic degradation of organic pollutants can be CO_2, H_2O and relevant inorganic ions. In order to evaluate the mineralization extent of MO, the TOC of MO solution was tested. Fig. 8 shows the mineralization ratio of
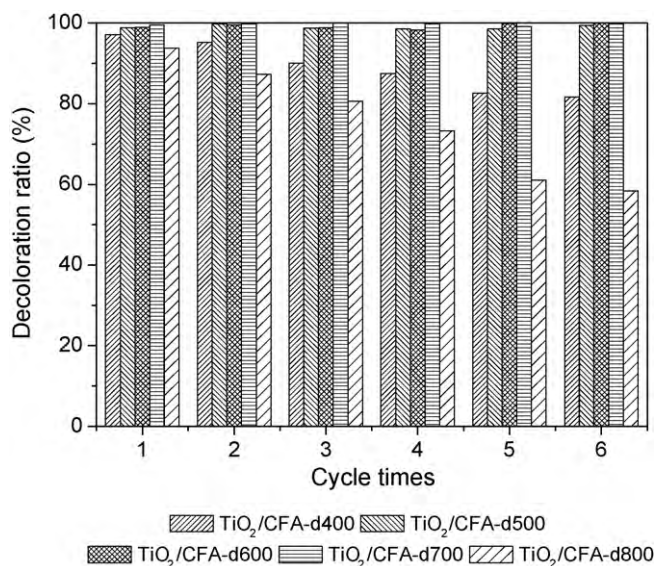
Fig. 7. Decoloration ratio of MO solution versus cycle times.

MO solution after 40 min under UV light irradiation with six times cycles. The mineralization ratio was calculated by using the same formula described in our early article [20]. We can also find that the mineralization ratio by using TiO_2/CFA-d400 or TiO_2/CFA-d800 as photocatalyst decreases gradually with the increase in the cycle times. Comparing with TiO_2/CFA-d700, the mineralization ratios of MO by using TiO_2/CFA calcined at 500 and 600 °C as photocatalysts are also slightly decline, which means 700 °C is the optimum calcination temperature for TiO_2/CFA photocatalyst to obtain the highest mineralization ratio and the optimal re-use property.

4. Discussion

The photocatalytic activity of TiO_2/CFA photocatalyst is governed by many factors, such as: (a) crystallization and crystal phase, (b) specific surface area, (c) crystal size of TiO_2, (d) light absorption characteristic and (e) mechanical stability.
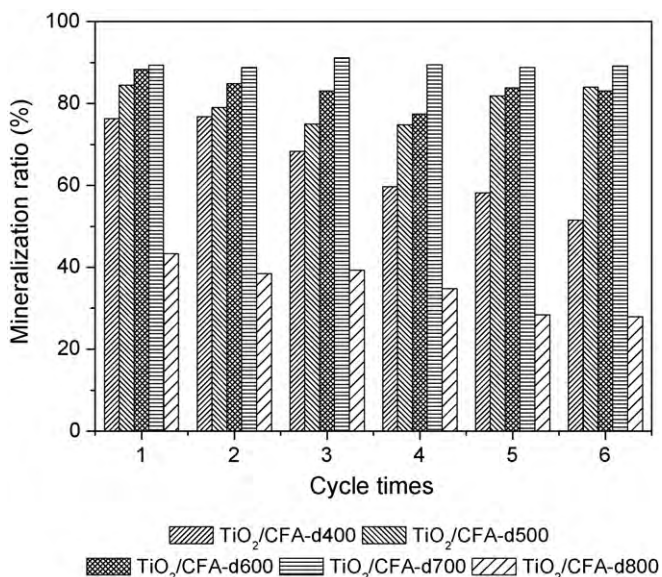

Fig. 8. Mineralization ratio of MO solution versus cycle times.

4.1. Crystallization and crystal phase

Crystallization plays a very important role in the photocatalytic activity of TiO_2. A better crystallization means the decrease of crystal defects, which are the recombination centers of photo-induced charge carries [46–51]. Therefore, in a sense, the improvement in photocatalytic activity of TiO_2 can be achieved by increasing the crystallization of TiO_2 [34,52–54], while, enhancing calcination temperature is one of methods to improve the crystallization of TiO_2 [52,55]. In current work, the maximum photocatalytic activity observed at 700 °C (see Fig. 6) indicates that the crystallization of TiO_2 is the dominating factor in determination the photocatalytic activity of TiO_2/CFA. Many other researched results also revealed the importance of crystallization in the photocatalytic behavior of catalysts [25,52,55]. The photocatalytic activity of samples increases significantly with the increase in calcination temperature from 400 to 700 °C, which can be ascribed to the fact that the crystallization of TiO_2 anchored on CFA increases with the increase in calcination temperature. This indicates that the negative effect induced from the decrease in surface area is compensated with the positive effect provided from the increase in the crystallization of TiO_2. TiO_2/CFA-d400 possesses the largest specific surface area, the smallest crystal size and the highest absorption capacity among the other TiO_2/CFA samples loaded with 49.97% TiO_2, but its photocatalytic activity is lower, the reason may be due to its worse crystallization, which can be deduced from its XRD pattern.

Besides, the crystal phase of TiO_2 is also an important factor for the photocatalytic activity. TiO_2 has three kinds of crystal phases, brookite, anatase and rutile. Among the three crystal phases, anatase and rutile are the most studied phases. Anatase is generally considered to be the active component based on the comparison between anatase and rutile [56–58]. There are some rutile phases in TiO_2/CFA calcined at 800 °C (see Fig. 2), which may be one of the reasons that TiO_2/CFA-d800 presents a low efficiency of photocatalytic decoloration [34,59].

4.2. Specific surface area

Although the increase in crystallization is considered as the major reason why the photocatalytic activity is improved by elevating the calcination temperature from 400 to 700 °C, the changes in the specific surface area of photocatalyst as varying calcination temperature also play a key role in determining the photocatalytic activity because the heterogeneous photocatalysis is a surface phenomenon [60–62]. Sample with larger specific surface area can pre-adsorb more MO molecules on the surface of sample, which helps to reduce the recombination of photogenerated electron and hole, and improves the efficiency of photocatalytic degradation [36]. Furthermore, the surface area can be correlated with the number of effective active sites. The increase of surface area means the increase of active sites on which MO molecules and intermediate products can adsorb [33,63]. Therefore, the enhancement of the specific surface area is one of methods for the increase of photocatalytic activity. The other reason why TiO_2/CFA calcined at 800 °C presents a low photocatalytic activity may be attributed to its low specific surface area resulted from the high calcination temperature. From Table 1, we can see that the specific surface area of TiO_2/CFA decreases with the increase in calcination temperature. So the specific surface area of TiO_2/CFA can be improved by decreasing the calcination temperature. However, low calcination temperature is not conducive to obtaining a good crystallization, which is very important to the photocatalytic activity of TiO_2/CFA. Therefore, how to improve the surface area of TiO_2/CFA photocatalyst on the basis of maintaining a good crystallization may be a good and promising attempt in the future.

4.3. Crystal size of TiO$_2$

The crystal size of catalyst particles is also an important factor for the photocatalytic activity [29]. Usually, smaller TiO$_2$ crystal size is favorable in photocatalytic reaction [64]. Firstly, smaller crystal size means larger surface area, which can provide more active sites for reactants adsorption. Secondly, to get a high photocatalytic activity, the photoexcited electron/hole pairs should effectively be migrated to the surface of catalyst and take part in the oxidation/reduction reaction before their recombination. So, the migrated distance greatly affects the utilization efficiency of photoexcited electron/hole pairs. Smaller crystal size means shorter distance that photoexcited electron/hole pairs should migrate, which reduces the recombination probability of electron/hole pairs and improves the photocatalytic activity of TiO$_2$. From Table 1, we have learned that with the increase in calcination temperature, the crystal size of TiO$_2$ also increases, which is detrimental to photocatalytic activity of TiO$_2$. TiO$_2$/CFA calcined at 800 °C presents a low photocatalytic activity, which may be correlated with the significant increase in its crystal size because of the phase transformation from anatase to rutile. If we reduce the crystal size of TiO$_2$ by decreasing the calcination temperature, the crystallization of TiO$_2$ will be bound to be affected. So, in the premise of maintaining a good crystallization of TiO$_2$, every effort to reduce the crystal size of TiO$_2$ may be worthy of devoting in the future.

4.4. Light absorption characteristic

It is well known that light absorption characteristic of photocatalyst is also an important factor that influences photocatalytic activity. The enhancement of absorbance in the UV–vis region increases the number of photogenerated electrons and holes to participate in the photocatalytic reaction, which can enhance the photocatalytic activity of TiO$_2$ [39,65]. So, the photocatalytic activity of TiO$_2$/CFA increases with the increase in calcination temperature from 400 to 700 °C, which may partly be attributed the fact that the absorption edge of the TiO$_2$/CFA samples increases with the increase in calcination temperature.

4.5. Mechanical stability

The mechanical stability is a very important issue, which directly relates to the using life of the supported catalyst. If the mechanical stability is poor, photocatalyst will gradually flake away from the substrate into the reaction solution during the using process [66], which not only leads the supported catalyst to lost photocatalytic activity prematurely, but also causes secondary pollution and the waste of catalyst. Some investigated results showed the mechanical stability is correlated with calcination temperature [33,67]. Generally speaking, increasing calcination temperature results in an enhancement of mechanical stability, and there is an optimal calcination temperature for the maximal mechanical stability. The poor recycling properties of TiO$_2$/CFA-d400 and TiO$_2$/CFA-d800 may be correlated with their poor mechanical stability because some TiO$_2$ particles broken away from the surface of CFA were removed from the reactive bottle after finishing a cycle, so the photocatalytic activity of TiO$_2$/CFA decreased gradually.

5. Conclusions

A batch of TiO$_2$/CFA samples calcined at different temperature was prepared by hybrid slurry procedure. The effects of calcination temperature on the structural property, photocatalytic activity and re-use performance of TiO$_2$/CFA photocatalysts were investigated in detail. From the above experimental results and discussion, it can be concluded that:

(1) With the increase in calcination temperature from 400 to 700 °C, many factors also increased, such as crystallization of TiO$_2$ adhered on the surface of CFA, the crystal size of TiO$_2$, mechanical stability, the absorption edges of the TiO$_2$/CFA samples, the efficiency of photocatalytic decoloration and mineralization. While, the specific surface area of TiO$_2$/CFA samples decreased with the increase in calcination temperature.

(2) Although the increase in calcination temperature could improve the photocatalytic activity of TiO$_2$/CFA. However, when calcination temperature was too high (800 °C), many negative factors would appear. we believe that 700 °C is the optimum calcination temperature for obtaining the optimal photocatalytic activity and re-use property under the conditions investigated in this study, and the reasons most probably due to the combined effects of many factors, such as the crystallization, the specific surface area, the crystal size, light absorption characteristic and mechanical stability.

Acknowledgements

References

[1] A. Zaleska, E. Grabowska, J.W. Sobczak, M.A Gazda, J. Hupka, Appl. Catal. B 89 (2009) 469–475.
[2] P. Pichat, J. Disdier, C. Hoang-Van, D. Mas, G. Goutailler, C. Gaysse, Catal. Today 63 (2000) 363–369.
[3] R.V. Grieken, J. Marugán, C. Sordo, P. Martínez, C. Pablos, Appl. Catal. B 93 (2009) 112–118.
[4] B. Zielinska, J. Grzechulska, A.W. Morawski, J. Photochem. Photobiol. A 157 (2003) 65–70.
[5] A. Rachel, M. Subrahmanyamb, P. Boule, Appl. Catal. B 37 (2002) 301–308.
[6] I. Mazzarino, P. Piccinini, Chem. Eng. Sci. 54 (1999) 3107–3111.
[7] J.-W. Shi, J.-T. Zheng, P. Wu, X.-J. Ji, Catal. Commun. 9 (2008) 1846–1850.
[8] P. Fu, Y. Luan, X. Dai, J. Mol. Catal. A 221 (2004) 81–88.
[9] C. Sarantopoulos, A.N. Gleizes, F. Maury, Thin Solid Films 518 (2009) 1299–1303.
[10] T. Yazawa, F. Machida, N. Kubo, T. Jin, Ceram. Int. 35 (2009) 3321–3325.
[11] A.R. Khataee, M.N. Pons, O. Zahraa, J. Hazard. Mater. 168 (2009) 451–457.
[12] M. Huang, C. Xu, Z. Wu, Y. Huang, J. Lin, J. Wu, Dyes Pigments 77 (2008) 327–334.
[13] H. Yahiro, T. Miyamoto, N. Watanabe, H. Yamaura, Catal. Today 120 (2007) 158–162.
[14] P. Pucher, M. Benmami, R. Azouani, G. Krammer, K. Chhor, J.-F. Bocquet, A.V. Kanaev, Appl. Catal. A 332 (2007) 297–303.
[15] O.K. Park, Y.S. Kang, Colloid Surf. A 257–258 (2005) 261–265.
[16] L. Ravichandran, K. Selvam, M. Swaminathan, J. Mol. Catal. A 317 (2010) 89–96.
[17] X. Cao, Y. Oda, F. Shiraishi, Chem. Eng. J. 156 (2010) 98–105.
[18] X. Querol, N. Moreno, J.C. Umaña, A. Alastuey, E. Hernández, A. López-Soler, F. Plana, Int. J. Coal Geol. 50 (2002) 413–423.
[19] R. Juan, S. Hernández, J.M. Andrés, C. Ruiz, Fuel 86 (2007) 1811–1821.
[20] J.-W. Shi, S.-H. Chen, S.-M. Wang, P. Wu, G.-H. Xu, J. Mol. Catal. A 303 (2009) 141–147.
[21] M. Zhang, Z. Jin, J. Zhang, Z. Zhang, H. Dang, J. Mol. Catal. A 225 (2005) 59–63.
[22] C. Guillard, B. Beaugiraud, C. Dutriez, J.-M. Herrmann, H. Jaffrezic, N. Jaffrezic-Renault, M. Lacroix, Appl. Catal. B: Environ. 39 (2002) 331–342.
[23] P. Gorska, A. Zaleska, E. Kowalska, T. Klimczuk, J.W. Sobczak, E. Skwarek, W. Janusz, J. Hupka, Appl. Catal. B 84 (2008) 440–447.
[24] Y.C. Dong, X.Q. Liu, Q.L. Ma, G. Meng, J. Membr. Sci. 285 (2006) 173–181.
[25] G. Colón, M.C. Hidalgo, J.A. Navío, Appl. Catal. A 231 (2002) 185–199.
[26] X. Zhang, K. Udagawa, Z. Liu, S. Nishimoto, C. Xu, Y. Liu, H. Sakai, M. Abe, T. Murakami, A. Fujishma, J. Photochem. Photobiol. A 202 (2009) 39–47.
[27] Y.T. Yu, Powder Technol. 146 (2004) 154–159.
[28] Q. Xiao, L. Ouyang, Chem. Eng. J. 148 (2009) 248–253.
[29] H. Wang, Z. Wu, Y. Liu, J. Hazard. Mater. 164 (2009) 600–608.
[30] J. Yu, H. Yu, B. Cheng, C. Trapalis, J. Mol. Catal. A 249 (2006) 135–142.
[31] C.-K. Lee, C.-C. Wang, M.-D. Lyu, L.-C. Juang, S.-S. Liu, S.-H. Hung, J. Colloid Interface Sci. 316 (2007) 562–569.
[32] G. Li, Z.-Q. Liu, J. Lu, L. Wang, Z. Zhang, Appl. Surf. Sci. 255 (2009) 7323–7328.
[33] Y. Chen, D.D. Dionysiou, J. Mol. Catal. A 244 (2006) 73–82.

[34] J.G. Yu, H.G. Yu, B. Cheng, X.J. Zhao, J.C. Yu, W.K. Ho, J. Phys. Chem. B 107 (2003) 13871–13879.
[35] T.K. Kim, M.N. Lee, S.H. Lee, Y.C. Park, C.K. Jung, J.H. Boo, Thin Solid Films 475 (2005) 171–177.
[36] J.-W. Shi, J.-T. Zheng, P. Wu, J. Hazard. Mater. 161 (2009) 416–422.
[37] L. Gomathi Devi, B. Narasimha Murthy, S. Girish Kumar, J. Mol. Catal. A 308 (2009) 174–181.
[38] J.G. Yu, M.H. Zhou, B. Cheng, X.J. Zhao, J. Mol. Catal. A 246 (2006) 176–184.
[39] M. Hamadanian, A. Reisi-Vanani, A. Majedi, Appl. Surf. Sci. 256 (2010) 1837–1844.
[40] D.R. Sahu, L.Y. Hong, S.-C. Wang, J.-L. Huang, Micropor. Mesopor. Mater. 117 (2009) 640–649.
[41] M. Hamadanian, A. Reisi-Vanani, A. Majedi, Mater. Chem. Phys. 116 (2009) 376–382.
[42] T. Lopez, F. Rojas, R. Alexander-Katz, F. Galindo, A. Balankin, A. Buljan, J. Solid State Chem. 177 (2004) 1873–1885.
[43] T. Sreethawong, Y. Yamada, T. Kobayashi, S. Yoshikawa, J. Mol. Catal. A 241 (2005) 23–32.
[44] M. Zhou, J. Yu, S. Liu, P. Zhai, L. Jiang, J. Hazard. Mater. 154 (2008) 1141–1148.
[45] J. Yu, L. Qi, B. Cheng, X. Zhao, J. Hazard. Mater. 160 (2008) 621–628.
[46] H.G. Yu, J.G. Yu, B. Cheng, J. Lin, J. Hazard. Mater. 147 (2007) 581–587.
[47] J.G. Yu, G.H. Wang, B. Cheng, M.H. Zhou, Appl. Catal. B 69 (2007) 171–180.
[48] J.G. Yu, J.F. Xiong, B. Cheng, S.W. Liu, Appl. Catal. B 60 (2005) 211–221.
[49] M. Mrowetz, W. Balcerski, A.J. Colussi, M.R. Hoffmann, J. Phys. Chem. B 108 (2004) 17269–17273.
[50] K.Y. Jung, S.B. Park, Korean J. Chem. Eng. 18 (2001) 879–888.
[51] L. Jing, Y. Qu, B. Wang, S. Li, B. Jiang, L. Yang, W. Fu, H. Fu, J. Sun, Solar Energy Mater. Solar Cells 90 (2006) 1773–1787.
[52] H. Wang, Y. Wu, B.-Q. Xu, Appl. Catal. B 59 (2005) 139–146.
[53] J. Ovenstone, J. Mater. Sci. 36 (2001) 1325–1329.
[54] H. Kominami, J. Kato, S. Murakami, Y. Ishii, M. Kohno, K. Yabutani, T. Yamamoto, Y. Kera, M. Inoue, T. Inui, B. Ohtani, Catal. Today 84 (2003) 181–189.
[55] M. Salmi, N. Tkachenko, V. Vehmanen, R.-J. Lamminmäki, S. Karvinen, H. Lemmetyinen, J. Photochem. Photobiol. A 163 (2004) 395–401.
[56] G.H. Li, L. Chen, M.E. Graham, K.A. Gray, J. Mol. Catal. A: Chem. 275 (2007) 30–35.
[57] J. Zhang, T. Ayusawa, M. Minagawa, K. Kinugawa, H. Yamashita, M. Matsuoka, M. Anpo, J. Catal. 198 (2001) 1–8.
[58] J. Zhu, W. Zheng, B. He, J. Zhang, M. Anpo, J. Mol. Catal. A 216 (2004) 35–43.
[59] Y. Tanaka, M. Suganuma, J. Sol–Gel Sci. Technol. 22 (2001) 83–89.
[60] X.F. You, F. Chen, J.L. Zhang, J. Sol–Gel Sci. Technol. 34 (2005) 181–187.
[61] S.-C. Jung, S.-J. Kim, N. Imaishi, Y.-I. Cho, Appl. Catal. B: Environ. 55 (2005) 253–257.
[62] L. Zhang, Y.F. Zhu, Y. He, W. Li, H.B. Sun, Appl. Catal. B: Environ. 40 (2003) 287–292.
[63] K.Y. Jung, S.B. Park, M. Anpo, J. Photochem. Photobiol. A 170 (2005) 247–252.
[64] T.A. Gad-Allah, K. Fujimura, S. Kato, S. Satokawa, T. Kojima, J. Hazard. Mater. 154 (2008) 572–577.
[65] D. Li, H. Haneda, S. Hishita, N. Ohashi, Mater. Sci. Eng. B 117 (2005) 67–75.
[66] K.V. Rao, M. Subrahmanyam, P. Boule, Appl. Catal. B 49 (2004) 239–249.
[67] H. Kim, S. Lee, Y. Han, J. Park, J. Mater. Sci. 40 (2005) 5295–5298.